中国光学（中英文） Chinese Optics 核心期刊

Continuous displacement measurement of large spot with stitched gratings

WANG Bo, WANG Wei, YIN Zhi-yu, WANG Xin-yu, LIU Zhao-wu, LI Wen-hao, GAO Xu, LIU Lin

Citation:
WANG Bo, WANG Wei, YIN Zhi-yu, WANG Xin-yu, LIU Zhao-wu, LI Wen-hao, GAO Xu, LIU Lin. Continuous displacement measurement of large spot with stitched gratings[J]. *Chinese Optics*, In press. doi: 10.37188/CO.EN-2025-0023
王博, 王玮, 尹志宇, 王新宇, 刘兆武, 李文昊, 高旭, 刘林. 拼接光栅的大光斑连续位移测量[J]. 中国光学, 优先发表. doi: 10.37188/CO.EN-2025-0023

View online: https://doi.org/10.37188/CO.EN-2025-0023

文章编号　2097-1842(xxxx)x-0001-12

Continuous displacement measurement of large spot with stitched gratings

WANG Bo[1,2], WANG Wei[1], YIN Zhi-yu[1], WANG Xin-yu[1], LIU Zhao-wu[1], LI Wen-hao[1], GAO Xu[3], LIU Lin[1*]

(1. *Changchun Institute of Optics, Fine Mechanics and Physics, Chinese Academy of Sciences, Changchun, Jilin* 130033, *China*;
2. *University of Chinese Academy of Sciences, Beijing* 100049, *China*;
3. *College of Optoelectronic Engineering, Changchun University of Science and Technology, Changchun* 130022, *Jilin, China*)

* *Corresponding author, E-mail: liulin@ciomp.ac.cn*

Abstract: Stitched gratings provide an important method to extend the grating displacement measurement range. However, the existence of stitched seams and stitching errors prevents high-precision continuous displacement measurement. This paper proposes an improved stitched grating displacement measurement method. The method reduces light signal intensity loss during stitching via a large spot suppression technique, ensures continuous displacement measurement using wavefront gradient modulation technology, establishes a theoretical model of the mapping between the stitched grating wavefront and the displacement measurement error, and verifies continuous displacement measurements experimentally using a single-sided Littrow optical path. Experimental results show that, based on the premise of matching the wavefront gradient index, the linear correlation between the theoretical model error and the actual measurement residual is greater than 0.9, and the corrected continuous displacement measurement residual is less than 50 nm. This verifies that the proposed method can realize high-precision continuous displacement measurement and high-stability range extension in the grating displacement measurement field.

Key words: grating displacement measurement; grating interferometer; stitching grating; wavefront measurement

---

收稿日期:2025-03-21; **修订日期**:xxxx-xx-xx

基金项目:国家自然基金(No. 62435019, No. 52275554, No. U21A20509, No. 61227901); 中科院青年基金专项(No. YSBR-103); 中国科学院青年创新促进会 (No. 2021220)

Supported by the National Natural Science Foundation of (No. 62435019, No. 52275554, No. U21A20509, No. 61227901); CAS Project for Young Scientists in Basic Research (No. YSBR-103); Chinese Academy of Sciences Youth Innovation Promotion Association (No. 2021220)

拼接光栅的大光斑连续位移测量

王 博[1,2], 王 玮[1], 尹志宇[1], 王新宇[1], 刘兆武[1], 李文昊[1], 高 旭[3], 刘 林[1*]
（1. 中国科学院长春光学精密机械与物理研究所, 吉林 长春 130033;
2. 中国科学院大学, 北京 101408;
3. 长春理工大学 光电工程学院 吉林长春 130022）

摘要: 拼接光栅是实现光栅位移量程拓展的重要方法, 但拼缝和拼接误差的存在导致无法实现高精度连续的位移测量。因此, 本文提出一种改进的拼接光栅位移测量方法, 通过大光斑抑制方法减少拼缝过程中光信号强度的损失, 利用波前梯度调制技术保证连续位移测量, 建立拼接光栅波前与位移测量误差的映射理论模型, 并使用单侧利特罗光路进行连续位移测量实验验证。实验结果表明, 在满足波前梯度指标的前提下, 理论模型误差与实际测量残差之间线性相关度大于0.9, 修正后连续位移测量残差小于 50 nm。充分验证了该方法能够实现高精度连续位移测量, 高稳定的量程拓展, 为光栅位移测量领域提供了新的量程拓展思路。

关 键 词: 光栅位移测量; 光栅位移测量; 拼接光栅; 波前测量
中图分类号: **文献标志码:** A **doi:** 10.37188/CO.EN-2025-0023 **CSTR:** 32171.14.CO.EN-2025-0023

1 Introduction

In modern industrial systems, high-precision continuous displacement measurement systems are essential for semiconductor technology and advanced manufacturing. Such as photolithography equipment, large-range CMMs, and high-precision machine tools with long stroke. Laser interferometers are seriously affected by environmental disturbances.Grating interferometers, which offer high precision, stability, and environmental resistance, are used widely in this field[1-6]. Higher grating line density enhances the measurement accuracy, but production of large-sized, high-density gratings is costly and error-prone. Stitched gratings can extend the measurement range, but maintaining high precision during range extension remains a major challenge[7-14].

Current research on stitched grating displacement measurement is primarily focused on multi-read-head data stitching. For example, Li et al. proposed a dual-read-head method for one-dimensional short-stroke measurements, albeit with a limited stroke and significant errors[15]. Gao et al. introduced a four-read-head structure for two-dimensional long-stroke measurement that ensured data continuity However, these multi-readout head displacement measurement methods are structurally complex, cumbersome to assemble, and introduce significant errors into the data stitched.[16, 17]. These methods often overlooked the effects of stitching errors on continuous displacement measurement, which can lead to uncontrolled continuity and large displacement errors. Therefore, quantitative analysis of grating stitching indicators and reduction of stitching-induced errors will be crucial for realization of high-quality continuous displacement range extension.

This paper proposes a single-read-head stitched grating continuous displacement measurement method. The technique uses large-spot optical filtering to mitigate interference signal attenuation at the seams and wavefront gradient modulation to control any signal changes caused by stitching errors, thus enabling continuous measurement and range extension. Experiments using the Littrow optical path show that gratings that match the wavefront gradient index can achieve high-quality continuous displacement measurements, with displacement residuals that align well with theoretical expectations.

Experimental results validate the effectiveness and accuracy of the proposed method

2 Principle

2.1 Tolerance Theory for Continuous Measurement of Spliced Gratings

The grating interferometer operates by extracting the Doppler frequency-shifted phase from the interference signal to resolve displacements. The optical configuration, which uses a single-pass Littrow structure, is illustrated in Fig. 1(a). A collimated laser beam passes through a beam expander (BE) and is subsequently divided into two beams using a polarizing beam splitter (PBS). Beam 1 propagates toward the spliced grating and is reflected at the Littrow incidence angle, retracing its original path. A quarter-wave plate (QWP) modulates the polarization state of the reflected beam. Beam 2 is reflected by a reference mirror and is modulated similarly by another QWP before recombining with Beam 1 to generate interference. When the two beams interfere, the composite vector intensity formula is[18-20]:

$$I = A_1^2 + A_2^2 + 2A_1A_2 \cdot \cos\left[(r_1 - r_2)\boldsymbol{k} + (\varphi_1 - \varphi_2) - \left(4\pi m \frac{v}{d} t\right)\right] \quad , \quad (1)$$

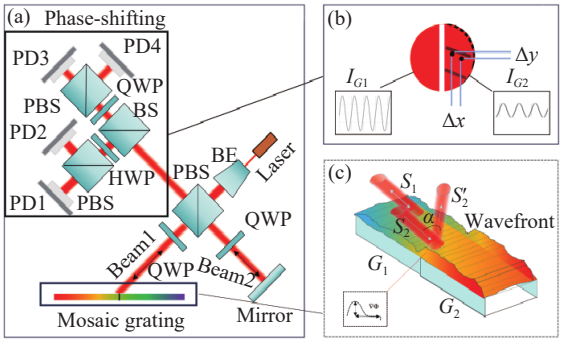

Fig. 1 Optical path and error impact. (a) Schematic of the optical path. (b) Variation of the optical interference signal. (c) Wavefront gradient and angular offset.

where A_1 and A_2 are the electric field intensities of the two light waves. The intensity I_{G2} of the interference light signal obtained from the two beams after passing through the grating varies with the angular error[21].

$$I_{G2} = \exp\left(-2\frac{L^2\alpha^2}{D^2}\right)\exp\left(\left(-\frac{(\sin\alpha)^2\pi^2D^2}{2\lambda^2}\right)\right) \cdot \{2A_1A_2 \cdot \cos[(\varphi_1 - \varphi_2) + \varphi_0]\} \quad , \quad (2)$$

where L is the optical path length, α is the overall diffraction angle deviation of grating G_2 relative to G_1, and D is the beam width.

During the grating diffraction propagation process, the wavefront gradient $\nabla\Phi$ describes the spatial rate of change of the phase surface on the grating.

$$\nabla\Phi = \sqrt{\left(\frac{\partial\phi}{\partial x}\right)^2 + \left(\frac{\partial\phi}{\partial y}\right)^2} \quad , \quad (3)$$

Where ϕ representative grating wavefront. For the diffraction direction perpendicular to the grating lines, which is conventionally designated as the x-direction in traditional gratings, it is assumed that the secondary waves emanating from each slit are coherent and exhibit uniform phase variation along the periodic structure. Under these conditions, the grating equation is expressed as:

$$d(\sin\theta_i + \sin\theta_d) = m\lambda \quad , \quad (4)$$

Where θ_i is the angle of incidence, and θ_d is the diffraction angle for the corresponding order.To achieve constructive interference, specifically the principal maximum, at a certain angle in the far field for secondary waves emitted from different positions, the sum of the phase differences caused by the angles of incidence and emergence, as well as the additional phase shifts due to the grating structure, phase difference φ introduced by the grating's wavefront error must be an integer multiple of 2π. Considering two adjacent points, the total phase difference between points x and $x+\Delta x$ is given by.

$$\Delta\varphi = \frac{2\pi}{\lambda}\sin\theta_i + [\varphi(x+\Delta x) - \varphi(x)] \quad , \quad (5)$$

Where Δx is a minute displacement element on the wavefront. The condition for coherent superposition demands that the phase difference between

these two parts is either zero or an integer multiple of $2m\pi$, that is:

$$k\sin\theta_d\Delta x = k\sin\theta_i\Delta x + [\varphi(x+\Delta x)-\varphi(x)] + 2\pi m \quad , \tag{6}$$

Where $k=\frac{2\pi}{\lambda}$ For the general case, considering the grating as having a continuous linear phase variation, we have:

$$\varphi(x+\Delta x)-\varphi(x) = \frac{\partial\phi}{\partial x}\cdot\Delta x \quad , \tag{7}$$

For m=0 or incorporating m into the total phase constant, eliminating Δxyields:

$$\sin\theta_d = \sin\theta_i + \frac{\Phi}{k} = \sin\theta_i + \frac{\lambda}{2\pi}\cdot\frac{\partial\phi}{\partial x} \quad , \tag{8}$$

The final modified grating diffraction condition is obtained as:

$$\theta_x \propto \frac{\partial\phi}{\partial x} \quad , \tag{9}$$

This implies that when the grating wavefront exhibits a non-zero gradient, the diffraction angle of the light beam θ_x relative to the incident light direction will be deflected, with the deflection being proportional to the phase gradient. For the y-direction, which is along the grating lines, the wavefront gradient is proportional to the beam exit direction, as previously reported in reference.

$$\theta_y \propto \frac{\partial\phi}{\partial y} \quad , \tag{10}$$

By solely examining the deflection caused by the beam's wavefront gradient, we can intuitively grasp the influence of stitching errors on the light deflection angle, and thereby infer their impact on the optical interference signal.

Because the diffraction propagation direction $\boldsymbol{S}$ is the same as the wavefront gradient direction for the corresponding grating order, the beam diffraction deflection angle and the wavefront gradient have the same spatial mapping, as shown in Fig. 1(c), which means that[22]:

$$\Delta\boldsymbol{S} = \alpha = \nabla\Phi \quad , \tag{11}$$

Where $\nabla\Phi=\left(\frac{\partial\varphi}{\partial x},\frac{\partial\varphi}{\partial y}\right)$ represents the gradient direction of the gratings. By measuring and adjusting the wavefront gradients of the stitched gratings, the angular distributions of the diffracted beams can be constrained, thus ensuring that the interference light meets the coherence criteria of the gratings. Let the contrast ratio be 1 when the light spot coincides completely with grating G_1, and let Q be the ratio of the light intensity when the light spot moves on grating G_2 to the corresponding intensity when it moves on grating G_1. Using $Q>0.9$ as the criterion, we derive the following relationship:

$$Q = \frac{\exp\left(-2\frac{(L\cdot\alpha)^2}{D^2}\right)\exp\left(\left(-\frac{(\sin\alpha)^2\pi^2D^2}{2\lambda^2}\right)\right)}{2A_1A_2\cdot\cos[(\varphi_1-\varphi_2)+\varphi_0]} \quad , \tag{12}$$
$$\{2A_1'A_2'\cdot\cos[(\varphi_1-\varphi_2)+\varphi_0)]$$

In the calculations, it is considered that $A_1=A_1'$ and that $A_2=A_2'$, and it is assumed that the gratings are in a mosaic condition. Because α is very small, we let $\sin\alpha$ be equivalent to α. From equations (11) and (12), we then obtain:

$$\nabla\Phi=\alpha=\sqrt{\frac{\ln(1/Q)\cdot 2\lambda^2D^2}{2L^2\lambda^2+D^4\pi^2}} \quad , \tag{13}$$

When the grating moves, the light frequency changes, and the expression for the light signal of the interference spot when moving at the seam can be simplified to read:

$$I_\delta = 2A_1A_2\cdot\cos\left[(\boldsymbol{k}\cdot(r_1-r_2)+(\varphi_1-\varphi_2)+4\pi m\frac{V}{d}\cdot t\right]+$$
$$2A_3A_4\cdot\cos\left[(\boldsymbol{k}\cdot(r_1-r_2)+(\varphi_1-\varphi_2)+4\pi m\frac{V}{d}\cdot t+\delta\right], \tag{14}$$

where A_3 and A_4 are the intensities of the two beams that enter stitched grating G_2.δ is the phase difference introduced by stitching.

2.2 Impact of Spot Size and Seam

To investigate the influence of varying spot sizes on intensity attenuation, numerical simulations were conducted to depict the light signal intensity distribution detected by the receiver under consistent light source output power and seam loss

width, yet with different spot diameters. During the simulation, the seam was deliberately positioned at the center of the Gaussian beam to induce the maximum intensity attenuation, which was subsequently contrasted with the anticipated attenuation outcomes. The results are illustrated in Fig. 2(a), 2(b), 2(c), and 2(d). The seam size was fixed at 0.8 mm, while the spot diameters in Fig. 2(a), 2(b), 2(c), and 2(d) were 6 mm, 9 mm, 12 mm, and 15 mm, respectively. A qualitative examination of these figures reveals that as the spot diameter expands, the loss of light signal intensity diminishes notably, and the overall light signal intensity captured and emitted by the detector correspondingly decreases. The ratio of the light intensity for different spot sizes to the light beam signal output intensity in the absence of a seam was computed. For spot sizes of 6 mm, 9 mm, 12 mm, and 15 mm, the ratios were 0.530, 0.723, 0.821, and 0.876, respectively.

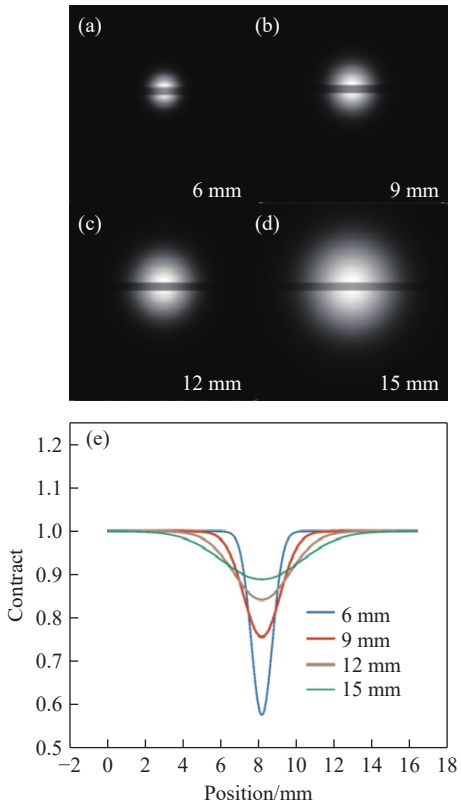

Fig. 2 Schematic diagram of the receiving end with different spot sizes (a) Light intensity diagram for a 6mm diameter spot(b) 9mm diameter spot(c) 12mm diameter spot(d) 15mm diameter spot(e) Intensity attenuation across different spot sizes

Leveraging the Gaussian formula, the impact of the spot-seam ratio on light signal intensity attenuation was graphically represented. As depicted in Fig. 2(e), the horizontal axis denotes the coordinate of the spot traversing the seam, with the simulation configured such that the seam is situated at the spot's center. The vertical axis signifies the ratio of the light intensity post-seam traversal, assuming the light intensity without any attenuation is unity. The blue, red, brown, and green lines correspond to the intensity attenuation for spot diameters of 6 mm, 9 mm, 12 mm, and 15 mm, respectively. A quantitative analysis of this simulation indicates that the minimum light signal intensity passing through the seam is 0.64, 0.75, 0.83, and 0.89 for the respective spot sizes. When the spot size exceeds 12 mm, the light intensity passing through the seam is assured to be above 0.83. At this juncture, provided that the stitching grating fulfills the contrast index of >0.9 stipulated in Section 2.1, the variation in light signal intensity aligns with the circuit calculation requirements, thereby enabling continuous displacement measurement. It should be noted that for large spots, the key focus is the spot-to-seam ratio. In this simulation, the spot-to-seam ratio is set to 15. If the seam becomes smaller, the spot size can be adjusted accordingly. Maintaining the spot-to-seam ratio ensures continuous signal measurement.

2.3 Impact of Beam Spot Size on Error Sensitivity

To elucidate the influence of varying beam spot diameters on error sensitivity, simulations were performed to examine the stitching error sensitivity for different beam spot sizes, as depicted in Fig. 3(a), (b), (c), and (d). The seam introduces intensity attenuation in the center of the beam spot. In the simulation, the beam spots above the seam are perfectly overlapping without any error, whereas there is a fixed angular deviation between the two beams below the seam. This angular deviation error between the two beams was set at 0.005°. With beam spot diameters set at 6 mm, 9 mm, 12 mm, and 15 mm, respectively, the analysis of these figures yields the following observations:

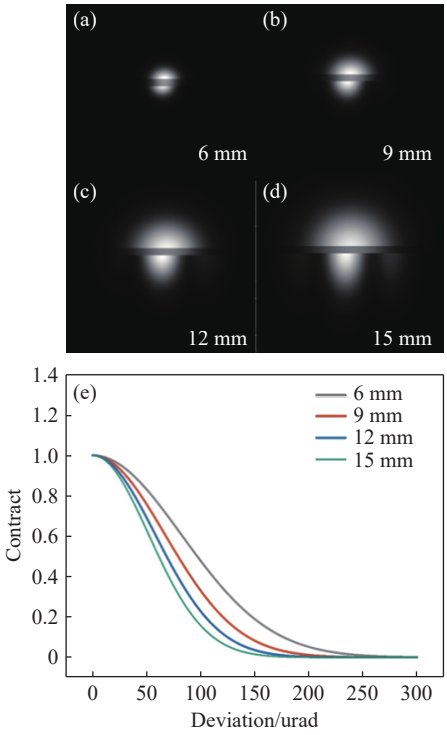

Fig. 3 Impact of Beam Spot Size on Error Sensitivity (a) Beam spot diameter 6 mm with a fixed tilt angle of 0.005° (b) 9 mm (c) 12 mm (d) 15 mm (e) Error sensitivity of different beam spots

In Fig. 3(a), the beam spot below the seam is partially offset relative to the beam spot above the seam.In Fig. 3(d), two dark fringes are observed in the beam spot below the seam compared to the beam spot above the seam.

The presence of more dark fringes correlates with a greater loss of optical interference signals. It is evident that, under the same angular deviation error, as the beam spot diameter increases, the loss of optical interference intensity progressively rises, and the attenuation ratio of optical signal intensity also increases. This implies a reduction in the contrast of the optical signal.

Fig. 3(e) presents a graph of beam spot size versus error sensitivity, derived from equation (13). The horizontal axis represents the beam angle deviation in degrees, while the vertical axis indicates the attenuation of optical signal intensity contrast. The gray, red, blue, and green lines in the figure correspond to the contrast attenuation curves for beam spots with diameters of 6 mm, 9 mm, 12 mm, and 15 mm, respectively, as the angle deviation varies. A qualitative analysis of the numerical curves reveals that as the beam spot diameter grows, the attenuation of optical signal contrast accelerates under the same beam angle deviation. This finding aligns with the aforementioned simulation results for the beam spot receiver.

Based on these simulation outcomes, it can be concluded that the beam spot size should not be excessively large, as this would result in a smaller allowable error limit for the grating angle to ensure continuous measurement. Comparing these results with those obtained in Section 2.2, the optimal beam spot diameter was selected. In the subsequent experiment, the beam spot diameter after expansion and collimation was chosen to be 12 mm. This size satisfies the requirements for optical intensity attenuation without causing significant attenuation of optical signal contrast.

2.4 Grating Stitching Wavefront Gradient and Contrast Mapping

To explore the influence of different stitching wavefront gradients on coherent intensity, simulations were conducted to examine the impact of various grating wavefront gradients on the coherent intensity detected by the receiver, as illustrated in Fig. 4(a), (b), (c), and (d). The distinct colors in these images signify varying intensity distributions. While the beam spot above the stitching is perfectly overlapping, the beam spot below the stitching shifts in accordance with the grating stitching wavefront. The wavefront gradients in these simulations were set at 0 nm/cm, 100 nm/cm, 200 nm/cm, and 300 nm/cm, respectively. The distribution of optical interference intensity on the detector is depicted in Fig. 4(a), (b), (c), and (d). As the grating stitching wavefront gradient increases from 0 nm/cm to 300 nm/cm, the dark fringes on the lower side of the stitching evolve from the absence of interference dark fringes in Fig. 4(a) to half a dark fringe within the beam spot in Fig. 4(d). The optical signal intensity received on the lower side of the stitching progressively diminishes, indicating that the contrast between the optical signal intensity on the lower side and the completely overlapping

wavefront optical signal intensity on the upper side gradually reduces.

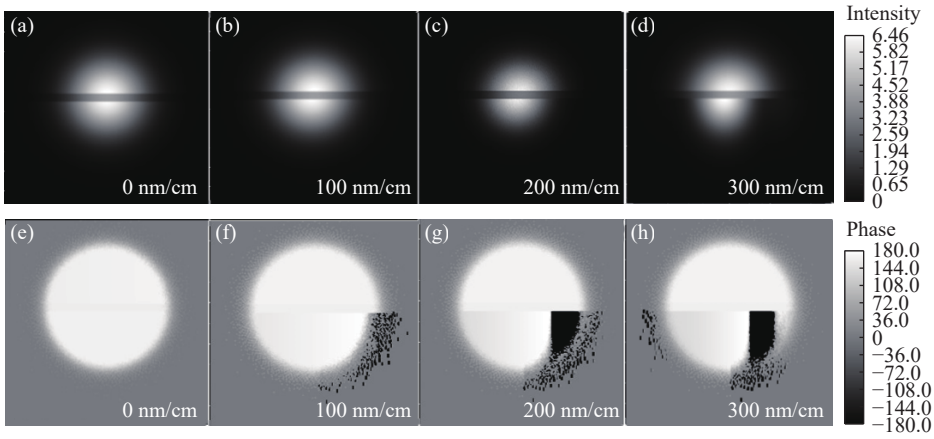

Fig. 4 Schematic diagrams of beam spots with different stitching wavefront gradients(a) Schematic diagram of optical 100 nm/cm (b) 200 nm/cm (c) 300 nm/cm (d) 400 nm/cm (e) Phase variation with a wavefront gradient of 100 nm/cm (f) 200 nm/cm (g) 300 nm/cm (h) 400 nm/cm

The simulation results of the interference phase of the beam spot under various grating wavefront gradients are depicted in Fig. 4(e), (f), (g), and (h). These images reveal that distinct wavefront gradients induce changes in the coherent phase detected by the detector. As the wavefront gradient escalates from 0 nm/cm to 300 nm/cm, the proportion of different phases within the optical coherence phase also progressively increases. The overall distribution of the optical coherence phase undergoes a significant shift, with −180° phase reversals emerging on both sides. This indicates that the overall phase of the lower beam spot has deviated. Consequently, as the grating wavefront gradient varies, an overall phase difference of the beam spot is introduced, and the phase of the optical interference signal detected at the detector end is disrupted. This disruption adversely affects the calculation of the measurement data.

2.5 Wavefront Error and Residual Mapping

Based on the aforementioned coefficients, a simulated plot of the wavefront gradient versus the contrast values was generated, as depicted in Fig. 5(a). The plot, in conjunction with the intensity change formula, clearly demonstrates that when the grating mosaic wavefront gradient is below 106 nm/cm, the contrast remains above 0.901 4. In subsequent grating mosaic calculations, the mosaic wavefront gradient tolerance required to ensure continuous measurement was set at 106 nm/cm, in accordance with the theoretical model.

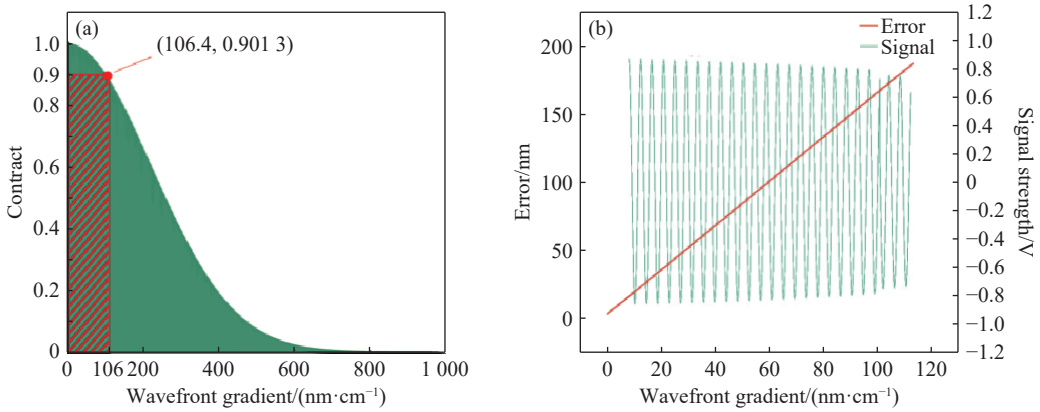

Fig. 5 Schematic diagram of wavefront gradient-related simulations (a) Simulation of wavefront gradient and contrast mapping (b) Simulation of wavefront gradient and error mapping

Simulations leveraging equation (14)were conducted to delineate the error curves introduced under various wavefront gradient error conditions, with an upper limit of 106 nm/cm, as illustrated in Fig. 5(b). The image reveals a linear mapping relationship between the wavefront gradient and the measurement residual. As the wavefront gradient escalates, the calculated residual correspondingly increases. Therefore, from a theoretical standpoint, the mosaic grating wavefront shape closely mirrors that of the actual measurement residual. Consequently, the error curve can be plotted based on the wavefront curve.

3 Experience and Results

We conducted displacement measurement experiments to verify this theory. During the displacement measurements, the laser interferometer (L-I) is used as the benchmark for the displacement measurement data. The beam spot size is 12 mm. The stitched grating was measured using the interferometer, and a two-dimensional displacement stage and a three-dimensional adjustment mechanism were used to adjust the wavefront.

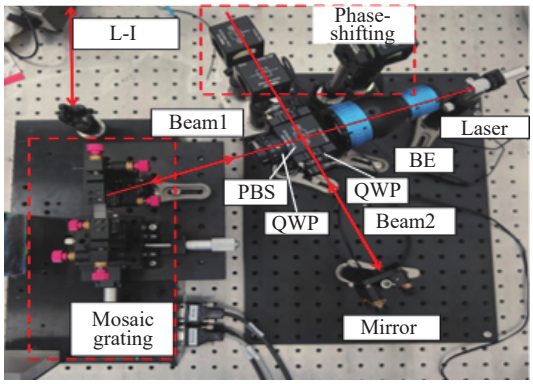

Fig. 6 Actual optical path diagram.

The results for the full grating surface wavefront measurements and the wavefront changes before and after stitching are shown in Fig. 7(a) and (c), respectively. They show that, without adjustment, the grating wavefront appears tilted and shifted. This will cause the beam diffraction directions on the two gratings to be inconsistent. After measurement and calculation, the wavefront gradient at the stitching was determined to be 325 nm/cm. By adjusting the grating using the interferometer, the wavefront measurement result was as shown in Fig. 7(c), where the wavefront for the two gratings is relatively flat, After measurement and calculation, the stitching wavefront error gradient was determined to be 65 nm/cm[23, 24].

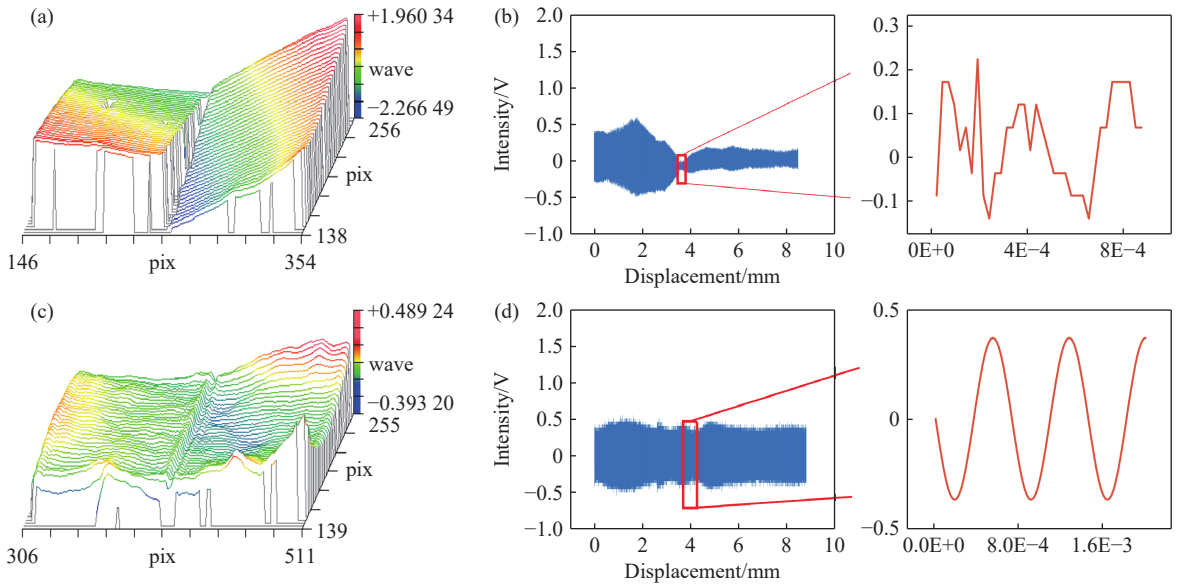

Fig. 7 Stitched wavefront maps and wavefront signal comparison diagrams. (a) Large stitched wavefront gradient map. (b) Large stitched wavefront signal schematic. (c) Small stitched wavefront gradient map. (d) Small stitched wavefront signal schematic.

The displacement stage was set to move at a speed of 2 mm/s. Because of the influence of the wavefront gradient, the interference signal intensity is inconsistent when the beam spot moves over the two gratings. As shown in Fig. 7(b), the contrast in the optical signal between G_2 and G_1 is 0.34. The interference signal at the stitching was amplified, and it was found that the sinusoidal and periodic nature of the interference signal had disappeared; thus, it could not meet the quality requirements of the continuous measurement signal. The grating displacement signal that meets the wavefront gradient stitching index requirements is shown in Fig. 7(d) with a contrast of 0.81, which meets the continuity requirements for the circuit solution. The sine signal observed at the stitching is good and is consistent with the expected results, which means that it can meet the conditions for continuous displacement measurement[25].

To verify the relationship between the wavefront gradient and the displacement measurement continuity, the displacement was measured at a speed of 2 mm/s for 8.5 mm at the grating stitching position. The displacement measurement data from the grating interferometer and the laser interferometer were plotted as shown in Fig. 8, where the horizontal axis represents the displacement position and the vertical axis represents the reference data of the interferometer (blue line) and the grating displacement data (red line). Fig. 8(a) shows a chart for comparison of the measurement data curve with a large wavefront gradient and the reference interferometer data. The curve shows that when the grating stitching wavefront error is large, signal loss will occur because of the stitching error, thus causing displacement data that should be linear to be interrupted. Fig. 8(b) shows a comparison chart for the measurement data curve with a small wavefront gradient and the reference interferometer, with only a small error between the two curves and no obvious interruption in the measurement data.

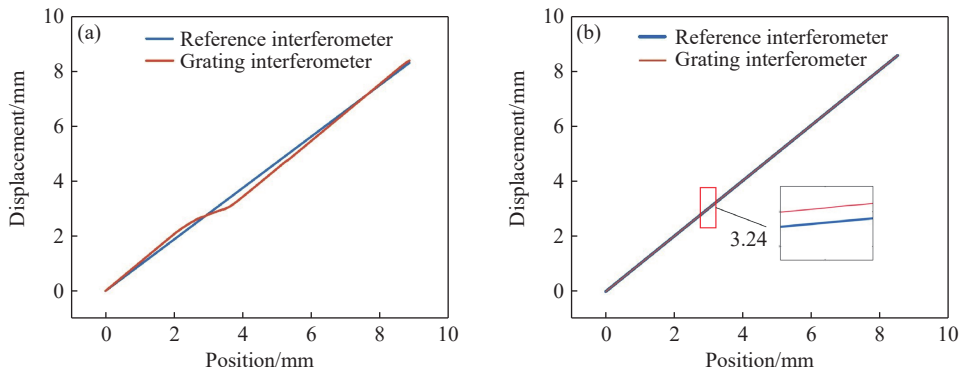

Fig. 8 Comparison of data from the grating interferometer and the laser interferometer. (a) Comparison of displacement residuals with large wavefront gradient and (b) with small wavefront gradient.

The stitched grating was fine-tuned to cause wavefront changes, and the wavefront error and the displacement residuals of groups 2 and 3 were measured. The wavefront gradients at the stitching for groups 1, 2, and 3 were 65 nm/cm, 86 nm/cm, and 95 nm/cm, respectively. The displacement stage was set to move to measure the data above, with displacement distances of 8.5 mm, 12 mm, and 12 mm, respectively.

The displacement residual curve for a large wavefront gradient is shown in Fig. 9(a), where a data loss situation occurs at the stitching, and the residual is extremely large before and after the beam spot passes through the stitching, with the full-range residual reaching 2.943 mm. Fig. 9(b), (c), and (d) show the residual distributions that meet the wavefront gradient index, where the red line is the error value calculated using the theoretical model (equation (14)); the data source is the wavefront error of the grating stitching displacement range obtained

via the interferometer, the blue line represents the residual data distribution obtained based on the difference between the grating interferometer and the laser interferometer, and the brown line represents the data fitted based on the residual data. Comparison of the brown line with the red line shows that there is strong correspondence between the residual fitting and the wavefront calculation error.

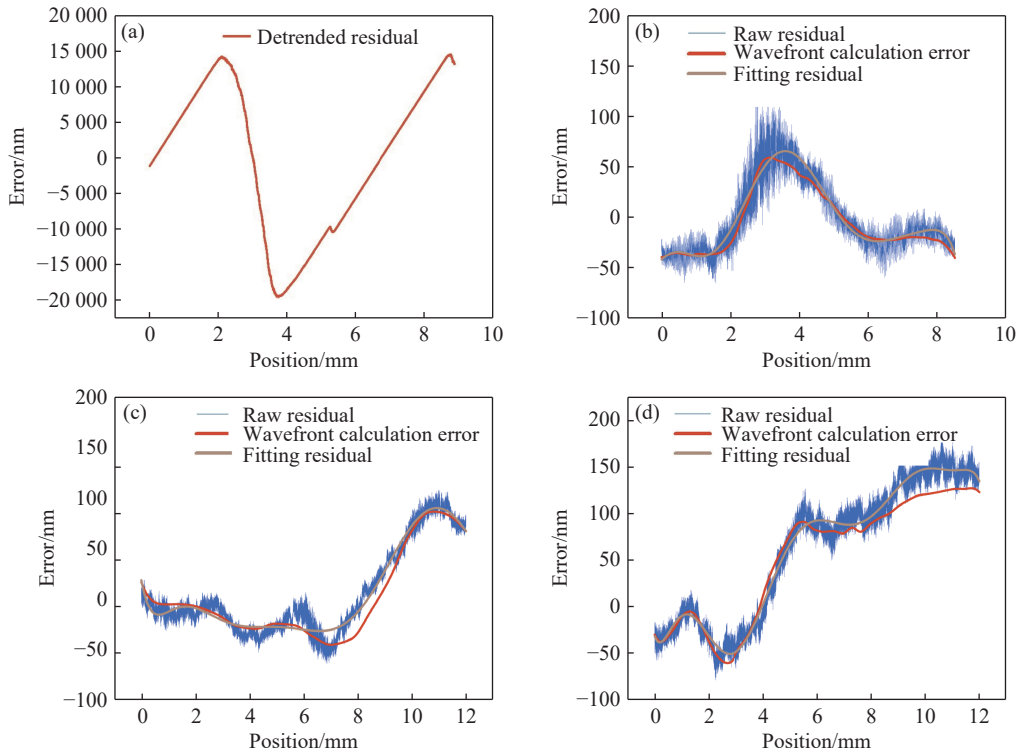

Fig. 9 Wavefront displacement residuals. (a) Displacement residual diagram that does not meet the wavefront index requirements. Displacement residual diagrams of (b) Group 1, (c) Group 2, and (d) Group 3.

A quantitative numerical analysis of the measured residual values and the theoretically calculated values was conducted. The measured residual error jump before and after the stitching was 109.01 nm, whereas the calculated stitching error jump was 101.3 nm, with the overall error fluctuating between −53 nm and 81 nm. The measured jump at the stitching for group 2 was 148 nm, and the calculated stitching error jump was 131.8 nm; the error fluctuated between −62 nm and 98 nm within the range. The measured fitted jump for group 3 was 157.6 nm, and the calculated stitching error jump was 149.4 nm, with the overall error fluctuating between −68 nm and 157 nm.

The linear correlation between the wavefront calculation error and the displacement error is greater than 0.9 for the different groups when calculated using different methods[26].

Tab. 1 Linear Correlation Relationship between Residuals and the Calculated Curve

	Group 1	Group 2	Group 3
Pearson	0.912 7	0.913 5	0.952 7
Spearman	0.903 5	0.967 2	0w.9084

The residuals were corrected using the wavefront calculation error data obtained from equation (14), with the error values being calculated from the wavefront at the displacement measurement data position, and an interpolation was performed after calculation for correction. Fig. 10 shows the error characteristics of the three error data groups after correction.

The errors were corrected from a maximum of 94.01 nm to 42.1 nm in group 1, from a maximum of 91.4 nm to 37.3 nm in group 2, and from a max-

imum of 157.4 nm to 38.5 nm in group 3, with a significant correction effect. Additionally, the nonlinear trend related to the stitched grating wavefront error in the displacement residual almost disappeared, and the experimental results show that the aim of using the stitching grating to perform high-precision continuous displacement measurement was achieved.

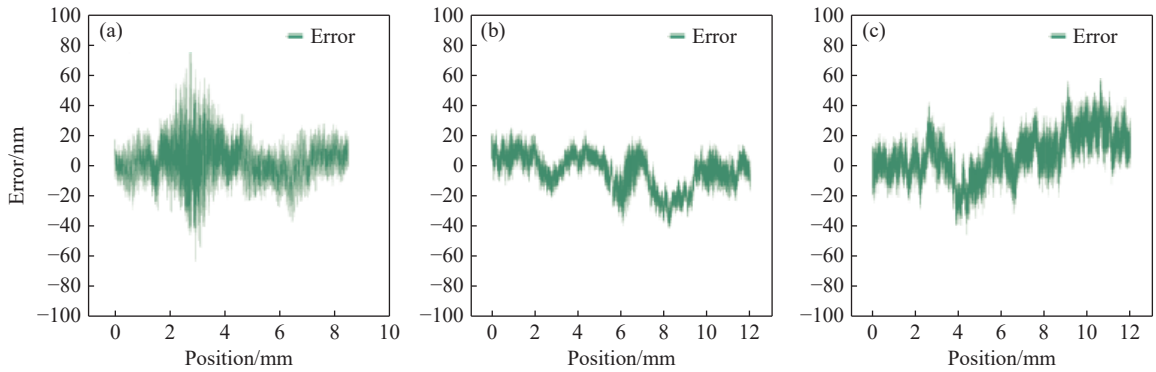

Fig. 10 Error characteristics of the three groups after correction. (a) Group 1, (b) Group 2, and (c) Group 3.

4 Conclusion

In summary, we proposed a high-precision continuous displacement measurement method for stitched gratings. The method uses a large beam spot for stitched grating interference displacement measurements and changes the wavefront gradient to ensure measurement continuity. The experimental displacement error was corrected using the wavefront calculation error and a significant correction effect was achieved. The results demonstrate that the wavefront gradient index calculated using the theoretical model guides continuous displacement measurements effectively, with a corrected error of less than 50 nm. This study provides theoretical support and experimental evidence for grating displacement measurement technology advancement.

References:

[1] GUO SH P, LU Z F, XIONG ZH, *et al*.. Lithographic pattern quality enhancement of DMD lithography with spatiotemporal modulated technology[J]. *Optics Letters*, 2021, 46(6): 1377-1380.

[2] ZHU CH, ZHUANG Y Y, LIU B, *et al*.. Review of fiber optic displacement sensors[J]. *IEEE Transactions on Instrumentation and Measurement*, 2022, 71: 7008212.

[3] HU P CH, CHANG D, TAN J B, *et al*.. Displacement measuring grating interferometer: a review[J]. *Frontiers of Information Technology & Electronic Engineering*, 2019, 20(5): 631-654.

[4] YU H Y, CHEN X L, LIU CH J, *et al*.. A survey on the grating based optical position encoder[J]. *Optics & Laser Technology*, 2021, 143: 107352.

[5] ZHOU W Y, SUN Y J, LIU ZH W, *et al*.. A random angle error interference eliminating method for grating interferometry measurement based on symmetry littrow structure[J]. *Laser & Photonics Reviews*, 2025, 19(11): 2401659.

[6] LI W H, WANG X Y, BAYANHESHIG, *et al*.. Controlling the wavefront aberration of a large-aperture and high-precision holographic diffraction grating[J]. *Light*: *Science & Applications*, 2025, 14(1): 112.

[7] HUANG Q SH, JIA Q, FENG J T, *et al*.. Realization of wafer-scale nanogratings with sub-50 nm period through vacancy epitaxy[J]. *Nature Communications*, 2019, 10(1): 2437.

[8] LIU ZH W, JIANG SH, LI X T, *et al*.. Precision measurement of X-axis stage mirror profile in scanning beam interference lithography by three-probe system based on bidirectional integration model[J]. *Optics Express*, 2017, 25(9): 10312-10321.

[9] BEYE M. Transient gratings with X-rays[J]. *Nature Photonics*, 2021, 15(7): 490-492.

[10] ZHANG J W, JIRIGALANTU, YU SH, *et al*.. Research on manufacturing technology of nanoimprinted grating[J]. *Journal of Manufacturing Processes*, 2024, 131: 891-909.

[11] WANG SH W, ZENG L J. Analysis and minimization of spacing error of holographic gratings recorded with spherical collimation lenses[J]. *Optics Express*, 2015, 23(5): 5532-5546.

[12] 卢禹先, 齐向东, 糜小涛, 等. 基于波前法的光栅拼接误差检测及计算方法[J]. 光学学报, 2016, 36(5): 0505001.
LU Y X, QI X D, MI X T, *et al*.. Detection and calculation of mosaic grating error based on wavefront method[J]. *Acta Optica Sinica*, 2016, 36(5): 0505001. (in Chinese).

[13] ZHOU H Y, ZENG L J. Optical mosaic method for orthogonally crossed gratings by utilizing information about both main periodic directions simultaneously[J]. *Optics Communications*, 2017, 385: 181-187.

[14] 钱国林, 吴建宏, 李朝明. 全息光栅并列拼接法的研究[J]. 光学学报, 2022, 42(21): 2105002.
QIAN G L, WU J H, LI CH M. Parallel splicing method for holographic gratings[J]. *Acta Optica Sinica*, 2022, 42(21): 2105002. (in Chinese).

[15] LI X H, YUAN W H, NI K, *et al*.. A two-probe linear encoder by using an arrayed scale grating stitched by multiple separate short gratings[J]. *Proceedings of SPIE*, 2018, 11053: 110530V.

[16] KIMURA A, GAO W, KIM W, *et al*.. A sub-nanometric three-axis surface encoder with short-period planar gratings for stage motion measurement[J]. *Precision Engineering*, 2012, 36(4): 576-585.

[17] SHIMIZU Y, ITO T, LI X H, *et al*.. Design and testing of a four-probe optical sensor head for three-axis surface encoder with a mosaic scale grating[J]. *Measurement Science and Technology*, 2014, 25(9): 094002.

[18] LIU L, LIU ZH W, JIANG SH, *et al*.. Polarization-modulated grating interferometer by conical diffraction[J]. *Optics Express*, 2022, 30(2): 689-699.

[19] SHA Q M, QIU S, LIU T, *et al*.. Doppler effect of polarization grating[J]. *Applied Optics*, 2021, 60(10): 2788-2794.

[20] KONKOLA P T. *Design and analysis of a scanning beam interference lithography system for patterning gratings with nanometer-level distortions*[D]. Cambridge: Massachusetts Institute of Technology, 2003.

[21] ZHOU W Y, LIU ZH W, SUN Y J, *et al*.. Corrigendum to "Bidirectional Littrow double grating interferometry for quadruple optical interpolation"[Opt. Laser Technol. 175 (2024) 110751][J]. *Optics & Laser Technology*, 2025, 181: 111974.

[22] BORN M. *Principles of Optics: Electromagnetic Theory of Propagation Interference and Diffraction of Light*[M]. London: Pergamon Press, 1959. **(查阅网上资料, 未能确认本条文献修改是否正确, 请确认)**.

[23] GAO W, KIMURA A. A fast evaluation method for pitch deviation and out-of-flatness of a planar scale grating[J]. *CIRP Annals*, 2010, 59(1): 505-508.

[24] PALMER C, LOEWEN E. *Diffraction Grating Handbook*[M]. 6th ed. Newport Corporation, 2005. **(查阅网上资料, 未找到出版地信息, 请补充)**.

[25] ZHOU W Y, SUN Y J, LIU ZH W, *et al*.. A random angle error interference eliminating method for grating interferometry measurement based on symmetry littrow structure[J]. *Laser & Photonics Reviews*, 2025, 19(11): 2401659. **(查阅网上资料, 本条文献和第 5 条文献重复, 请核对)**.

[26] LI L F, QIU K Q, CHEN H Y. Method to overlay an interference field over a grating using only the grating's profile symmetry[J]. *Optics Letters*, 2024, 49(11): 2906-2909.

Author Biographies:

WANG Bo (1999—), male, born in Song-Yuan, JiLin Province, master student. Changchun Institute of Optics, Fine Mechanics and Physics, Chinese Academy of Sciences. His research interests are on Grating displacement measurement. E-mail: 2544766835@qq.com

LIU Lin (1996—), male, born in Changchun, JiLin Province, Ph.D, Changchun Institute of Optics, Fine Mechanics and Physics, Chinese Academy of Sciences. Her research interests are on Grating interferometer. E-mail: liulin@ciomp.ac.cn